A substrate descriptor based approach for the prediction and understanding of the regioselectivity in caged catalyzed hydroformylation†

Pim R. Linnebank, [ID] *[a] David A. Poole, [ID] [a] Alexander M. Kluwer[b] and Joost N. H. Reek [ID] *[ab]

The use of data driven tools to predict the selectivity of homogeneous catalysts has received considerable attention in the past years. In these studies often the catalyst structure is varied, but the use of substrate descriptors to rationalize the catalytic outcome is relatively unexplored. To study whether this may be an effective tool, we investigated both an encapsulated and a non-encapsulated rhodium based catalyst in the hydroformylation reaction of 41 terminal alkenes. For the non-encapsulated catalyst, **CAT2**, the regioselectivity of the acquired substrate scope could be predicted with high accuracy using the Δ^{13}C NMR shift of the alkene carbon atoms as a descriptor ($R^2 = 0.74$) and when combined with a computed intensity of the C=C stretch vibration ($I_{\text{C=C stretch}}$) the accuracy increased further ($R^2 = 0.86$). In contrast, a substrate descriptor approach with an encapsulated catalyst, **CAT1**, appeared more challenging indicating a confined space effect. We investigated Sterimol parameters of the substrates as well as computer-aided drug design descriptors of the substrates, but these parameters did not result in a predictive formula. The most accurate substrate descriptor based prediction was made with the Δ^{13}C NMR shift and $I_{\text{C=C stretch}}$ ($R^2 = 0.52$), suggestive of the involvement of CH–π interactions. To further understand the confined space effect of **CAT1**, we focused on the subset of 21 allylbenzene derivatives to investigate predictive parameters unique for this subset. These results showed the inclusion of a charge parameter of the aryl ring improved the regioselectivity predictions, which is in agreement with our assessment that noncovalent interactions between the phenyl ring of the cage and the aryl ring of the substrate are relevant for the regioselectivity outcome. However, the correlation is still weak ($R^2 = 0.36$) and as such we are investigating novel parameters that should improve the overall regioselectivity outcome.

[a]Homogeneous, Supramolecular and Bio-Inspired Catalysis, Van't Hoff Institute for Molecular Sciences, University of Amsterdam, Science Park 904, 1098 XH Amsterdam, The Netherlands. E-mail: j.n.h.reek@uva.nl; p.r.linnebank@uva.nl

[b]InCatT B.V., Science Park 904, 1098 XH Amsterdam, The Netherlands

† Electronic supplementary information (ESI) available. See DOI: **https://doi.org/10.1039/d3fd00023k**
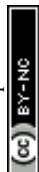
Introduction

Enzymes have served as major sources of inspiration for synthetic chemists, as such systems offer levels of selectivity control unattainable using traditional transition metals. Through multiple interactions between the substrate and the enzyme, the regio-, enantio- and chemoselectivity can be controlled for otherwise unselective reactions. As such, several commonplace elements used by enzymes such as a confined space and/or noncovalent interactions have been consciously incorporated into the design of transition metal catalysts.[1–15] This has been achieved by incorporating hydrogen bond donors and/or acceptors into the ligand structure to, similar to enzymes, achieve higher selectivity.[1,12,13] Alternatively transition metal catalysts have been encapsulated into supramolecular cages to mimic the confined spaces commonly observed in enzymes and the application of encapsulated transition metal catalysts has led to impressive examples of selectivity control for several reactions.[16–37]

Due to the complex shapes of encapsulated catalysts, a small variation in the substrate structure can lead to large variations in the overall catalytic outcome and the catalytic outcome of a single substrate cannot be easily extrapolated to other substrates. Despite this fact, the substrate scope is often not explored extensively in reports discussing encapsulated transition metal catalysts.[17,28–31,38,39]

To rationalize the catalytic outcome, often DFT calculations combined with analytical techniques are used to rationalize catalytic outcomes and predict the selectivity for novel substrates.[40–47] To explain the catalytic outcomes using DFT calculations, all pathways need to be considered for every substrate. However, this is not feasible due to computational cost and computational resources required for large systems, such as when encapsulated transition metal catalysts are studied and/or large amounts of substrates are investigated. Because of this, the catalytic results are often only rationalized afterwards, and methods to predict how additional substrates would react often remain elusive. Therefore, it is desirable to find methods that circumvent elaborate DFT calculations, while being able to predict the catalytic outcome of a large substrate scope with reasonable accuracy.

Recently multivariate data driven approaches have been applied to predict the catalytic outcomes of catalyzed reactions.[3,48–60] These methods have received considerable attention as these require less computational power while providing valuable information about catalytic systems studied. To be successful, these methods typically require large data sets. Most often catalyst descriptors are used to devise a mathematical model that accurately describes the catalytic outcome for a range of catalysts for a reaction using the same substrates (Fig. 1). However, substrate descriptors should also be applicable to rationalize the catalytic outcome of a large substrate scope. This would then lead to mechanistic insights as such an approach should demonstrate what substrate moieties affect the
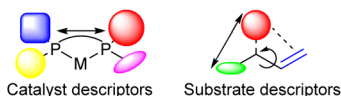

Fig. 1 Catalyst and substrate descriptors for the prediction of catalyst performance.
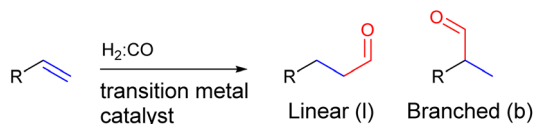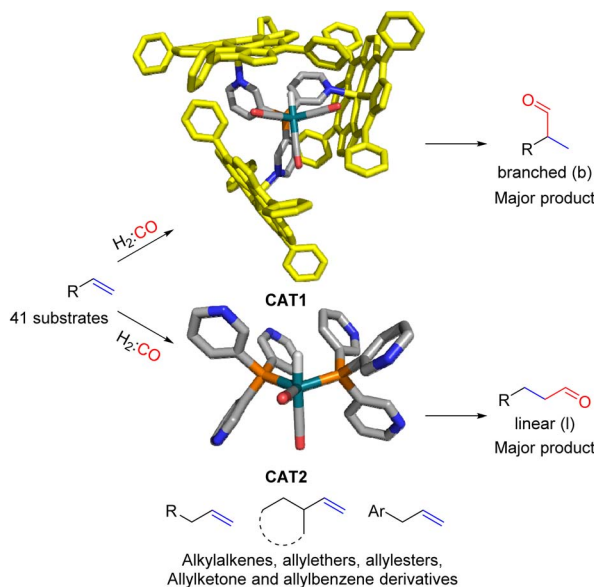
Fig. 2 General scheme of the hydroformylation reaction showing that two regio-isomers of the aldehyde product can be formed.

selectivity outcome, while the amount of computational resources required is lower as only the substrates have to be modeled.

In the hydroformylation reaction, syngas ($H_2 : CO$) is reacted with an alkene in the presence of a transition metal catalyst to form an aldehyde (Fig. 2). Since the aldehyde can add onto both sides of the alkene, a regio-isomeric mixture is typically formed and as such regioselectivity control is a longstanding challenge for this reaction.[61–63]

In our group we have reported an encapsulated hydroformylation catalyst based on rhodium using a ligand-template *meta*-tris pyridylphosphine ($P(_mPy_3)$) and three zinc-tetraphenylporphyrin (ZnTPP) building blocks (Scheme 1).[19,20]

The cage formation relies on the selective coordination of the ZnTPP building blocks to the pyridine moieties of the ligand-template $P(_mPy_3)$. $[Rh(H)(CO)_3(P(_mPy_3(ZnTPP))_3)]$ was the active catalyst which formed under syngas ($H_2 : CO$) conditions. This encapsulated catalyst offered unique regioselectivity in the hydroformylation reaction as this catalyst is able to convert terminal alkenes such as 1-octene to form an excess of the branched aldehyde (linear/branched ratio = 0.56) (Fig. 3). For internal alkenes, such as 2-octene, the innermost internal aldehyde (outermost/innermost ratio = 1/9) is dominantly formed.[21]

Scheme 1 Substrate scope investigation of the encapsulated $[Rh(H)(CO)_3(P(_mPy_3(-ZnTPP))_3)]$ catalyst (**CAT1**) in the hydroformylation reaction of terminal alkenes.

Faraday Discussions

Previous work

1-octene
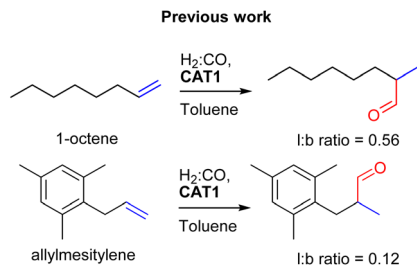
l:b ratio = 0.56

allylmesitylene

l:b ratio = 0.12

Fig. 3 Significant variation in the regioselectivity control with **CAT1**.

Recently, we evaluated the substrate scope of this caged catalyst ([Rh(H)(CO)$_3$(P($_m$Py$_3$(ZnTPP))$_3$)] (**CAT1**)) using 41 terminal alkenes and compared the outcomes against an unencapsulated reference catalyst [Rh(H)(CO)$_2$(P($_m$Py$_3$))$_2$] (**CAT2**) (Scheme 1).[64] For all substrates investigated, **CAT1** produces more branched product than **CAT2**. The degree of branched selectivity enhancement, however, significantly varies between substrates and no clear rationale was discovered for why certain substrates gave a significantly higher regioselectivity enhancement to the branched product than others (Fig. 3). To explain the catalytic outcomes using DFT calculations is not feasible due to computational cost and computational resources required due both to the size of **CAT1** as well as the size of the substrate scope.[22,65,66] We hypothesized that this data set could be used to apply a substrate descriptor based approach to uncover regioselectivity trends, which ultimately should lead to more insight into the cage effects induced by hydroformylation catalyst **CAT1**.

As descriptors, steric[53] and electronic parameters[54–56] as well as IR frequencies[57] have been used. These have been successfully applied to predict catalyst properties for several different reactions including organocatalyzed[52,58,59] and transition metal catalyzed reactions.[53–57,60] Based on a limited parameter set, a mathematical model is constructed. This model shows which parameters, such as steric or noncovalent interactions, largely affect the outcome of the reaction and this allows for the *a priori* identification of substrates that react with high selectivity with a chosen catalyst as well as entries towards improved catalyst design. An effective substrate descriptor approach for the investigated substrate scope would provide an important tool for identifying substrates that can be converted with high selectivity with a chosen encapsulated transition metal catalyst. Additionally, this could significantly reduce the amount of experiments required to identify reactions that are practically applicable.

Results and discussion

To investigate whether a substrate descriptor approach was able to accurately predict the regioselectivity, we used the catalytic results of the encapsulated [Rh(H)(CO)$_3$(P($_m$Py$_3$(ZnTPP))$_3$)] catalyst (**CAT1**) in the hydroformylation reaction of 41 terminal alkenes as a data set.[64] As a reference, the catalytic results of an unencapsulated [Rh(H)(CO)$_2$(P($_m$Py$_3$))$_2$] (**CAT2**) catalyst were used, which is the catalyst that is formed under the same conditions in the absence of the Zn–porphyrin building blocks. In all cases, two regioisomers were formed; the linear

(l) and the branched (b) aldehyde product (Fig. 2). Using the linear/branched ratios of all entries, we calculated the relative reaction barriers ($\Delta\Delta E$) for **CAT1** and **CAT2** based on the Boltzmann distribution with k_B being the Boltzmann constant and T being the reaction temperature in Kelvin:

$$\Delta\Delta E = \ln\left(\frac{\text{linear}}{\text{branched}} \text{ ratio}\right) \times k_B T \tag{1}$$

These experimentally determined energies were used to find correlations between substrate properties and the cage induced selectivity (expressed in relative energies between the product forming pathways).

Modeling of a non-encapsulated reference catalyst

We commenced our studies by modeling the catalytic results of **CAT2**, the unencapsulated catalyst. This was done to create a benchmark and gain insight into what parameters govern the regioselectivity for non-encapsulated catalysts where substrate rotation is not limited. For the substrate parametrization, the catalytic outcomes of **CAT2** were plotted against the polarization of alkene moieties of the substrates. It is well known that the polarization of the alkene plays a large role in determining the regioisomeric outcome in the hydroformylation reaction.[61,62,67–69]

As a physical parameter, the difference between the ^{13}C shift of the two olefinic carbon atoms ($\Delta^{13}C$ shift) was used and correlated to the selectivity of the hydroformylation reaction with **CAT2** (Fig. 4). In previous olefin insertion reactions, this has been identified as a descriptor that strongly correlates with the regioisomeric outcome.[55,56,69] Plotting the regioselectivity ($\Delta\Delta E$) against the $\Delta^{13}C$ shift of all substrates evaluated shows a relatively strong correlation with **CAT2**, demonstrating that for the unencapsulated **CAT2** the regioselectivity in the hydroformylation reaction can be predicted with a reasonable accuracy using the $\Delta^{13}C$ shift as a substrate descriptor, in line with a previous report.[69]
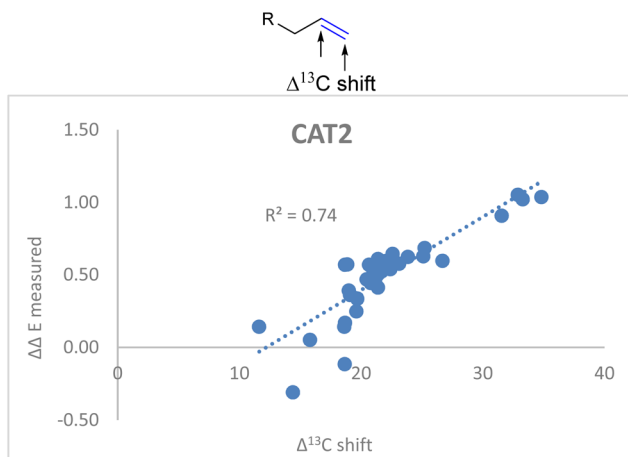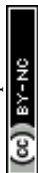

Fig. 4 Plot of the experimental regioselectivity expressed in $\Delta\Delta E$ against the $\Delta^{13}C$ shift for all substrates studied for the unencapsulated catalyst **CAT2**.
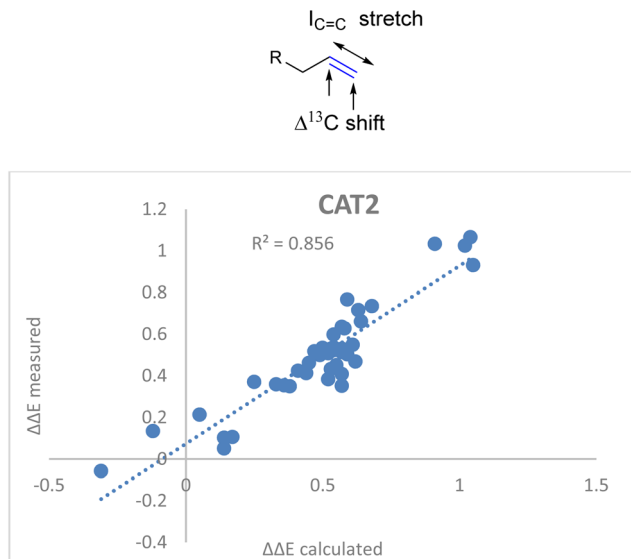
Fig. 5 Correlation plot of regioselectivity ($\Delta\Delta E_{CAT2}$) predicted *versus* the experimentally obtained regioselectivity using the $\Delta^{13}C$ shift and $I_{C=C\ stretch}$ substrate parameters as indicated in eqn (2).

To improve the accuracy of our predictions, we calculated the C=C IR-stretch intensity ($I_{C=C\ stretch}$) for all substrates using DFT calculations as this frequency was proven to be a useful descriptor that accurately predicts the selectivity for some other reactions.[52,57,58,70] This was done by calculating the lowest energy structures and subsequently using the Amsterdam Density Functional (ADF) program.[71–73] The B3LYP-D3(BJ)[74–76] density functional was used together with a small core TZ2P basis set for both the geometry optimizations as well as the frequency calculations.

$$\Delta\Delta E_{CAT2} = 0.038\Delta^{13}C_{shift} + 0.021I_{C=C\ stretch} - 0.70 \qquad (2)$$

Including the $I_{C=C\ stretch}$ in the descriptor formula led to a strong correlation ($R^2 = 0.86$) between the calculated and the observed regioselectivity (Fig. 5). The fact that the regioselectivity in the hydroformylation reaction can be predicted with high accuracy shows that the regioisomeric outcome with CAT2 is mostly governed by alkene polarization, as the IR intensity is mainly governed by the charge redistribution within the bond under specific vibrational transitions.[77]

Modeling of the encapsulated catalyst

Using the models of our non-encapsulated reference catalyst, CAT2, we pursued the modelling of CAT1. For all substrates evaluated, the encapsulated CAT1 provided more of the branched product than the unencapsulated CAT2. Therefore, a lower $\Delta\Delta E$ for all the reaction outcomes with CAT1 compared to CAT2 is obtained. With this energy value we subtracted the $\Delta\Delta E$ with CAT1 from the $\Delta\Delta E$ with CAT2 for every substrate which is a measure of the cage induced selectivity, coined the cage effect:
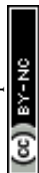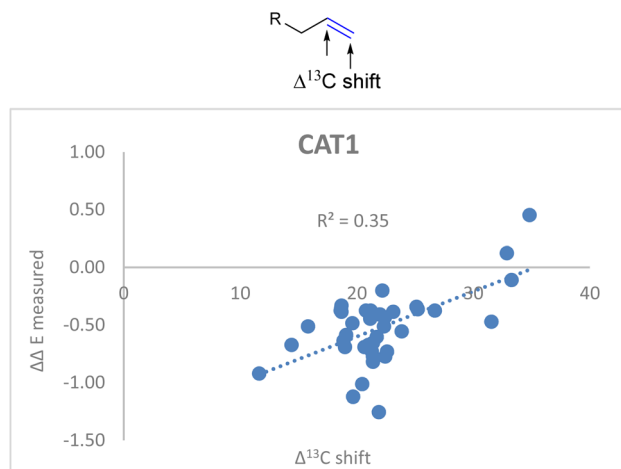
Fig. 6 Plot of the experimental regioselectivity expressed in $\Delta\Delta E$ against the $\Delta^{13}C$ shift for all substrates studied for the encapsulated catalyst **CAT1**.

$$\text{Cage effect} = \Delta\Delta E_{\textbf{CAT2}} - \Delta\Delta E_{\textbf{CAT1}} \tag{3}$$

This measure provides insight into what way the confined space affects the substrate's selectivity and corrects for inherent substrate bias. Since the **CAT1** provides a higher branched selectivity than **CAT2** for all substrates, all cage effects were positive.

Also for **CAT1** the regioselectivity induced by the catalyst was plotted against the $\Delta^{13}C$ shift (Fig. 6). Consistent with our expectations, the correlation was significantly less strong compared to **CAT2** using the same parameter (0.35 *vs.* 0.74).

This is in line with the anticipated effect of the confined space around **CAT1** as this interacts in a different way when the shape and/or the functional groups on the substrates are altered. Therefore, we hypothesized that models that account for the shape of the substrates could improve the predictive ability of our models. To obtain models that account for the shape of the substrates, we extended the substrate descriptors investigated to Sterimol parameters (Fig. 7), which are parameters that systematically account for the steric influence of the shape of the substrates as reported by Verloop *et al.*[78] Previous work reported by Sigman *et al.* has shown that for several reactions such descriptors are useful to account for steric effects of functional groups.[52–54,58]

We investigated whether such simple steric parameters can account for the interactions such substrates experience with the inner compartment of caged
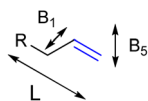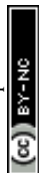

Fig. 7 Sterimol parameters acquired to find stronger correlations between substrate properties and selectivity in hydroformylation displayed by **CAT1**.

catalyst **CAT1**. Using the DFT calculated structures of the substrates, we obtained Sterimol parameters. The Sterimol values consist of two width parameters (B_1 and B_5) and a length parameter (L). The different width parameters were calculated according to the profile of the substituent when viewed down the axis of the C=C bond. B_1 is defined as the minimum width perpendicular to the primary bond axis. This value generally describes the extent of branching at the first carbon center next to the C=C bond. The B_5 parameter describes the maximum width orthogonal to the same axis, which is a degree for how wide the substrate is. L is the total length of the substituent along the C=C axis.
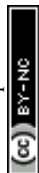
In the first instance, the substrate descriptor values were plotted against the regioselectivity of **CAT1** and **CAT2**. The cage effect (expressed in $\Delta\Delta E$) was also used and the overall R^2 values for every parameter are presented in Fig. 8.

These values show that better correlations are observed for **CAT2** than **CAT1** for most substrate descriptors. B_1 also correlates with the regioselectivity displayed by **CAT1**, however, construction of a multiparameter formula with B_1 does not result in improved fitting results. The inspection of the substrate scope shows that the B_1 parameter mostly reflects di-substitution ($B_1 \approx 2.4$) or mono-substitution ($B_1 \approx 1.8$) on the aliphatic carbon atom next to the alkene. However, di-substitution on this carbon atoms is also reflected strongly in $\Delta^{13}C$ shift where disubstituted alkenes have a significantly higher $\Delta^{13}C$ shift. This also results in a low orthogonality of this parameter to the $\Delta^{13}C$ shift, which in turn is reflected by a low correlation between B_1 and the cage effect.
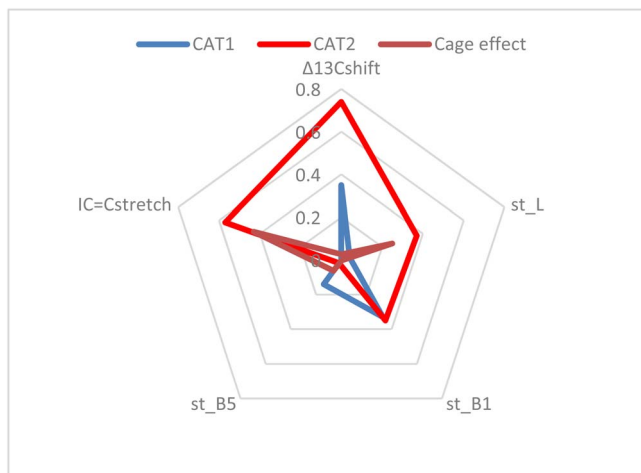
	$\Delta^{13}C$ shift	st_L	st_B_1	st_B_5	l$_{C=C\ stretch}$
CAT1	$R^2 = 0.35$	$R^2 = 0.041$	$R^2 = 0.33$	$R^2 = 0.14$	$R^2 = 0.0002$
CAT2	$R^2 = 0.74$	$R^2 = 0.37$	$R^2 = 0.35$	$R^2 = 0.018$	$R^2 = 0.57$
Cage effect	$R^2 = 0.027$	$R^2 = 0.25$	$R^2 = 0.0021$	$R^2 = 0.062$	$R^2 = 0.43$

Fig. 8 Correlation between descriptors and experimental results (given as R^2 values) and a visual representation of parameters investigated.
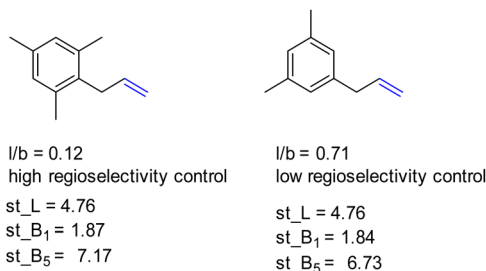
l/b = 0.12
high regioselectivity control

st_L = 4.76
st_B$_1$ = 1.87
st_B$_5$ = 7.17

l/b = 0.71
low regioselectivity control

st_L = 4.76
st_B$_1$ = 1.84
st_B$_5$ = 6.73

Fig. 9 Bulky substrates both display high regioselectivity control as well as low regioselectivity control with **CAT1** despite having similar Sterimol parameters.

Also, L, the substrate length parameter, and B_5, the parameter that represents the maximum width of the substrate orthogonal to the C=C bond, display low correlation values for both catalysts and do not provide useful handles to predict the regioselectivity displayed by these catalysts. Indeed, in our substrate scope investigation, some bulky substrates reacted with exceptionally high branched selectivity (e.g. allylmesitylene, l/b = 0.12) whereas other bulky substrates reacted with low branched selectivity (e.g. 3-(3,5-dimethylphenyl)-1-propene, l/b = 0.71) (Fig. 9), which exemplifies the limitations of employing Sterimol parameters for predicting the catalytic outcome with **CAT1**. Despite the low correlations observed, we explored correlation equations that included the Sterimol parameters. However, these did not yield significantly better correlations to describe the regioselectivity observed by **CAT1** and **CAT2** than the equation based on solely the Δ^{13}C shift. This shows that the interactions of the substrates with the cage cannot be simply accounted for with the Sterimol parameters. Most likely, the cage effect of **CAT1** involves the precise position of the substrate which is governed by steric hindrance in combination with noncovalent interactions.

As the confined space around **CAT1** resembles the active site of enzymes, we also explored substrate descriptors derived from computer-aided drug design (CADD) using RDKit (Fig. 10).[79] The substrate descriptors investigated included Kappa shape indices (κ_1, κ_2, κ_3),[80,81] Chi shape indices (χ_{0n-3n}, χ_{0v-3v}),[81] topological polar surface area (TPSA),[82] eccentricity,[83] plane of best fit (PBF),[84] asphericity,[85] sphericity, principal moments of inertia (PMI1, PMI2, PMI3, NPR1, NPR2), approximate surface area (LabuteASA), inertial shape factor (ISF),[85] spherocity index,[85] the number of rotatable bonds. Unfortunately, none of these substrate descriptors that we examined resulted in strong correlations for the regioselectivity outcomes of **CAT1**, **CAT2**, or the cage effect.

R / MD / 41 substrates → [R /] → κ_1, κ_2, κ_3, χ_{0n}, χ_{1n}, χ_{2n}, χ_{3n}, χ_{0v}, χ_{1v}, χ_{2v}, χ_{0n}, χ_{3v}, TPSA, PBF, Asphericity, PMI1, PMI2, PMI3, NPR1, NPR2, Spherocity index, NumRotable Bonds, NumConformers
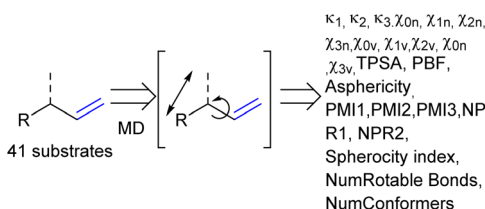
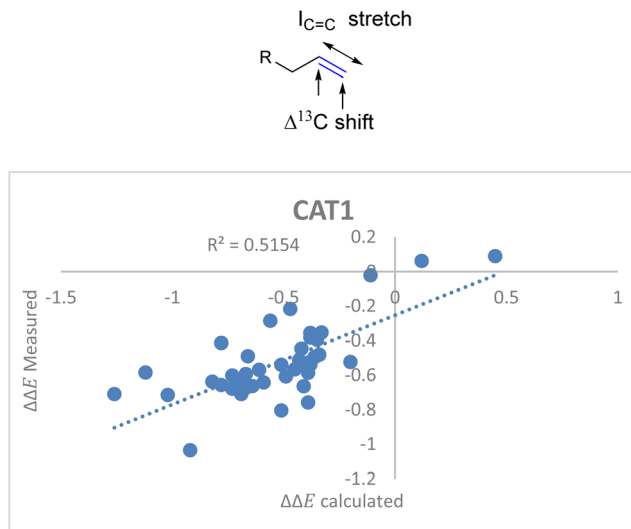**Fig. 10** Molecular dynamics calculations to acquire additional substrate descriptors.

Fig. 11 Moderate correlation for catalytic outcome with **CAT1** and the $\Delta^{13}C$ shift and $I_{C=C\ stretch}$ substrate parameters.

For the unencapsulated catalyst **CAT2** the correlation function significantly improved when the $I_{C=C\ stretch}$ was included. Also, this descriptor correlated well with the cage effect (Fig. 8) and therefore this descriptor was also explored for cage catalyst **CAT1**. With the $I_{C=C\ stretch}$ included as a substrate descriptor the overall fit for the selectivity displayed by **CAT1** indeed improved ($R^2 = 0.35$ vs. 0.52) (Fig. 11).

$$\Delta\Delta E_{\textbf{CAT1}} = 0.057\Delta^{13}C_{shift} - 0.031I_{C=C\ stretch} - 1.28 \qquad (4)$$

Surprisingly, the $I_{C=C\ stretch}$ had an opposite sign in the correlation equation for **CAT1** as a catalyst. The correlation equation for **CAT1** shows that an increase in $I_{C=C\ stretch}$ intensity enhances the selectivity for the branched product, whereas the correlation equation for **CAT2** predicts that a higher $I_{C=C\ stretch}$ intensity enhances the selectivity for the linear product. A plausible explanation is that the alkene
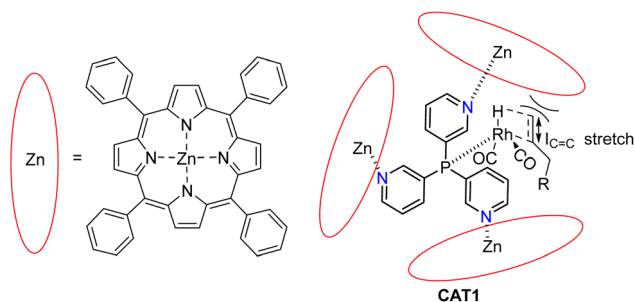

Fig. 12 Noncovalent interactions between the alkene moiety and aromatic plane of the cage affect the regioselectivity.

Paper

interacts with the aromatic planes of the walls of the cage as the alkene is in close proximity with the ZnTPP walls, which results in an altered $I_{C=C\ stretch}$ vibration (Fig. 12). Indeed, simple DFT calculations show that the intensity of the $I_{C=C\ stretch}$ is affected in the proximity of an aromatic surface. The regioselectivity predictions are still significantly less accurate for **CAT1** than **CAT2** ($R^2 = 0.51$ *vs.* 0.86), indicating that we didn't capture the cage effect to its full extent yet. Therefore, it is still desirable to acquire substrate and/or substrate/catalyst descriptors for the substrate scope with **CAT1** to construct a formula with higher accuracy.

Modeling of allylbenzene subsection with CAT1

Since we struggled to obtain parameters that accurately account for cage–substrate interactions for the entire substrate scope, we set out to acquire parameters with the allylbenzene subset (Fig. 13).

We chose this subset as it is the largest subset investigated and there is a significant variation in the overall regioselectivity outcome with **CAT1**, while the
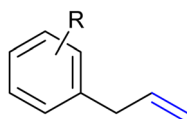
21 substrates
R = Me(1x,2x,3x), Cl,
Br, F(1x,5x),CF₃

Fig. 13 Allylbenzene subset investigated to understand the noncovalent interactions between **CAT1** and the substrates.
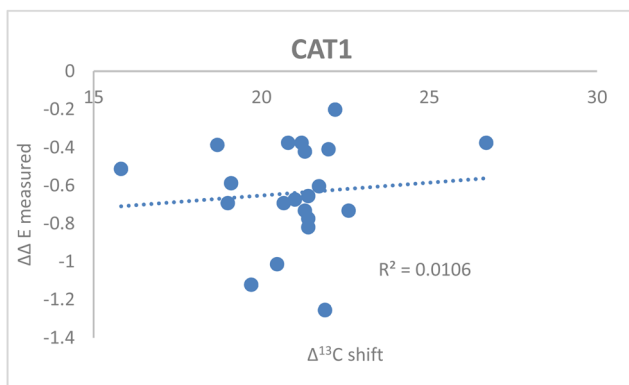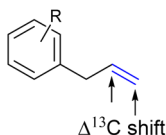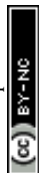

Fig. 14 Weak correlation between the alkene polarization (represented by Δ^{13}C shift) and the regioselectivity outcome of allylbenzene derivatives for **CAT1**.

alkene polarization is comparable for this substrate class. Furthermore, the difference in size between all the substrates does not explain the regioselectivity trends observed. Correlation equations have also been applied to a limited set of similar substrates in other reports.[53,54,56,70] This is generally more facile as the catalyst–substrate interactions are generally more similar, making the construction of predictive formulae less complicated. Possibly, due to the diversity of the substrates investigated in this study, the construction of a general formula that accounts for all substrates evaluated is unsuccessful for **CAT1**. Therefore, better correlations might be obtained with models that only cover certain substrate classes. However, the added value of such models is lower as the formulae only apply to a single class of substrates.

If the alkene polarization (Δ^{13}C shift) of all allylbenzene derivatives against measured $\Delta\Delta E$ is plotted, no correlation between the regioselectivity outcome and the alkene polarization of allylbenzene derivatives is observed ($R = 0.011$) (Fig. 14).

Since there was no correlation between the polarization of the alkenes and the overall regioselectivity outcome we investigated additional parameters to obtain a better correlation.

DFT calculations in previous reports show that the computed substrates (*i.e.* 2-octene and allylbenzene) display CH–π interactions with the porphyrin walls of the cage.[22,64] Since the aryl ring of **CAT1** interacted with the aryl ring of allylbenzene in a DFT study, we hypothesized that the charge of the aryl ring of the allylbenzene derivatives could provide a predictive parameter of the regioselectivity outcome as these interactions differ between substrates and are most likely responsible for the large differences in selectivity control, *e.g.*, the regioselectivity differences between the allylbenzene type substrates (*vide supra*).
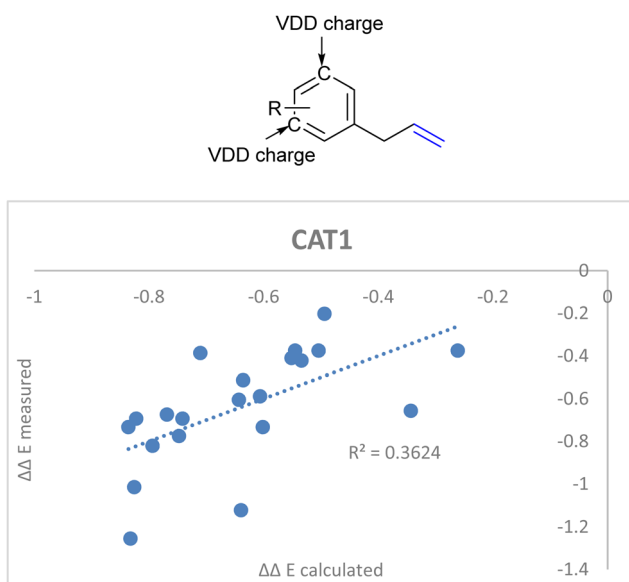

Fig. 15 Improved regioselectivity prediction of the allylbenzene derivative substrate scope with the inclusion of VDD charges on the *meta*-carbon atoms of the aryl rings.

Additionally, these substrates show interesting regioselectivity effects, where *ortho* and *para* substituents lead to an increased branched selectivity, whereas *meta* substituents lead to decreased branched selectivity. When combined with the aforementioned $I_{C=C\ stretch}$ we obtained a significantly better correlation when we included the average Voronoi deformation density (VDD) charge of the C3 and C5 positions of the aryl ring as an additional descriptor (Fig. 15, eqn (5)).[86] This is in agreement with our previously reported assessment that noncovalent interactions between the aryl ring of the allylbenzene moiety and the aryl ring of the ZnTPP moiety of the catalyst affect the regioselectivity.[22,64] It shows that a more negative charge on these positions lowers the $\Delta\Delta E$, which leads to a higher branched selectivity.

$$\Delta\Delta E_{\mathbf{CAT1}} = 0.062\Delta^{13}C_{shift} - 0.036I_{C=C\ stretch} + 2.92VDD_{meta} + 1.30 \qquad (5)$$

Similar to the formula that covered the entire substrate scope evaluated, inclusion of the Sterimol or CADD derived descriptors did not result in a significant improvement of the predictivity of the constructed mathematical equations. Recently Sigman *et al.* reported a workflow to predict the selectivity of a class of cavity shaped C–H activation catalysts accurately.[51] Several additional descriptors of the catalysts, coined SMART, were included to accurately predict the selectivity of these catalysts. The selectivity of the catalysts investigated in this study are also caused by confinement effects, similar to **CAT1**.

Conclusions

In this contribution we evaluated if substrate descriptors are useful to predict and understand the regioselectivity outcomes of a substrate scope in the hydroformylation reaction. To study this, an encapsulated catalyst **CAT1** and an unencapsulated reference catalyst **CAT2** were used to correlate the observed regioselectivity against equations based on different substrate descriptors. For the unencapsulated **CAT2**, a formula was constructed that described the catalytic outcome with high accuracy ($R^2 = 0.86$) using the $\Delta^{13}C$ shift of the alkenes and the $I_{C=C\ stretch}$ as substrate descriptors. This is in agreement with our assertion that the outcome is mostly determined by the alkene polarization parameters and remote substituents do not significantly affect the catalytic outcome with this catalyst.

A similar approach for the encapsulated catalyst **CAT1** showed that the selectivity of the reaction was significantly more difficult to predict and it is clear that additional substrate parameters such as steric interactions between the substrates and the cage as well as noncovalent interactions play a role in determining the overall regioselectivity. Sterimol and molecular dynamics derived parameters were investigated in order to improve the model by accounting for the substrate size. However, the use of such parameters does not lead to improved models for prediction of the selectivity of the reaction. The models used did not account for the noncovalent interactions displayed between substrate moieties and the walls of the cages as well as the relative flexibility of the substrate. As such, we investigated correlation equations using the allylbenzene derivative substrates subset when reacted with **CAT1** and found a significant improvement when we

included the average VDD charge at the C3 and C5 positions of the allylbenzene derivatives. Despite this improvement, the accuracy of the formula predicting the regioselectivity was still low using these descriptors ($R^2 = 0.36$). As such we are currently investigating additional parameters to be able to accurately predict the regioselectivity of substrates when reacted with **CAT1**.

Author contributions

PL conceived the project, wrote the manuscript and conducted the data analytical work. DP performed the CADD calculations. JR conceived the project, supervised the project and wrote the manuscript. AK helped write the manuscript.

Conflicts of interest

There are no conflicts to declare.

Acknowledgements

Notes and references

1 J. N. H. Reek, B. de Bruin, S. Pullen, T. J. Mooibroek, A. M. Kluwer and X. Caumes, *Chem. Rev.*, 2022, **122**, 12308–12369.
2 S. H. A. M. Leenders, R. Gramage-Doria, B. de Bruin and J. N. H. Reek, *Chem. Soc. Rev.*, 2015, **44**, 433–448.
3 F. D. Toste, M. S. Sigman and S. J. Miller, *Acc. Chem. Res.*, 2017, **50**, 609–615.
4 D. M. Vriezema, M. C. Aragonès, J. A. A. W. Elemans, J. J. L. M. Cornelissen, A. E. Rowan and R. J. M. Nolte, *Chem. Rev.*, 2005, **105**, 1445–1489.
5 M. Raynal, P. Ballester, A. Vidal-Ferran and P. W. N. M. van Leeuwen, *Chem. Soc. Rev.*, 2014, **43**, 1660–1733.
6 M. Raynal, P. Ballester, A. Vidal-Ferran and P. W. N. M. van Leeuwen, *Chem. Soc. Rev.*, 2014, **43**, 1734–1787.
7 M. J. Wiester, P. A. Ulmann and C. A. Mirkin, *Angew. Chem., Int. Ed.*, 2011, **50**, 114–137.
8 L. Catti, Q. Zhang and K. Tiefenbacher, *Chem.–Eur. J.*, 2016, **22**, 9060–9066.
9 R. J. Severinsen, G. J. Rowlands and P. G. Plieger, *J. Inclusion Phenom. Macrocyclic Chem.*, 2020, **96**, 29–42.
10 M. Morimoto, S. M. Bierschenk, K. T. Xia, R. G. Bergman, K. N. Raymond and F. D. Toste, *Nat. Catal.*, 2020, **3**, 969–984.
11 J. Meeuwissen and J. N. H. Reek, *Nat. Chem.*, 2010, **2**, 615–621.
12 P. Dydio and J. N. H. Reek, *Chem. Sci.*, 2014, **5**, 2135–2145.
13 H. J. Davis and R. J. Phipps, *Chem. Sci.*, 2017, **8**, 864–877.
14 L. J. Jongkind, X. Caumes, A. P. T. Hartendorp and J. N. H. Reek, *Acc. Chem. Res.*, 2018, **51**, 2115–2128.
15 S. S. Nurttila, P. R. Linnebank, T. Krachko and J. N. H. Reek, *ACS Catal.*, 2018, **8**, 3469–3488.
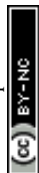
16 C. J. Brown, F. D. Toste, R. G. Bergman and K. N. Raymond, *Chem. Rev.*, 2015, **115**, 3012–3035.

17 T. Gadzikwa, R. Bellini, H. L. Dekker and J. N. H. Reek, *J. Am. Chem. Soc.*, 2012, **134**, 2860–2863.

18 C. García-Simón, R. Gramage-Doria, S. Raoufmoghaddam, T. Parella, M. Costas, X. Ribas and J. N. H. Reek, *J. Am. Chem. Soc.*, 2015, **137**, 2680–2687.

19 V. F. Slagt, J. N. H. Reek, P. C. J. Kamer and P. W. N. M. van Leeuwen, *Angew. Chem., Int. Ed.*, 2001, **40**, 4271–4274.

20 V. F. Slagt, P. C. J. Kamer, P. W. N. M. van Leeuwen and J. N. H. Reek, *J. Am. Chem. Soc.*, 2004, **126**, 1526–1536.

21 M. Kuil, T. Soltner, P. W. N. M. van Leeuwen and J. N. H. Reek, *J. Am. Chem. Soc.*, 2006, **128**, 11344–11345.

22 V. Bocokić, A. Kalkan, M. Lutz, A. L. Spek, D. T. Gryko and J. N. H. Reek, *Nat. Commun.*, 2013, **4**, 2670.

23 M. Jouffroy, R. Gramage-Doria, D. Armspach, D. Sémeril, W. Oberhauser, D. Matt and L. Toupet, *Angew. Chem., Int. Ed.*, 2014, **53**, 3937–3940.

24 X. Wang, S. S. Nurttila, W. I. Dzik, R. Becker, J. Rodgers and J. N. H. Reek, *Chem.–Eur. J.*, 2017, **23**, 14769–14777.

25 C. Gibson and J. Rebek, *Org. Lett.*, 2002, **4**, 1887–1890.

26 D. H. Leung, R. G. Bergman and K. N. Raymond, *J. Am. Chem. Soc.*, 2007, **129**, 2746–2747.

27 D. H. Leung, R. G. Bergman and K. N. Raymond, *J. Am. Chem. Soc.*, 2006, **128**, 9781–9797.

28 T. A. Bender, R. G. Bergman, K. N. Raymond and F. D. Toste, *J. Am. Chem. Soc.*, 2019, **141**, 11806–11810.

29 M. Otte, P. F. Kuijpers, O. Troeppner, I. Ivanović-Burmazović, J. N. H. Reek and B. de Bruin, *Chem.–Eur. J.*, 2014, **20**, 4880–4884.

30 M. Otte, P. F. Kuijpers, O. Troeppner, I. Ivanović-Burmazović, J. N. H. Reek and B. de Bruin, *Chem.–Eur. J.*, 2013, **19**, 10170–10178.

31 P. F. Kuijpers, M. Otte, M. Dürr, I. Ivanović-Burmazović, J. N. H. Reek and B. de Bruin, *ACS Catal.*, 2016, **6**, 3106–3112.

32 M. L. Merlau, M. D. P. Mejia, S. T. Nguyen and J. T. Hupp, *Angew. Chem., Int. Ed.*, 2001, **40**, 4239–4242.

33 J. L. Suk, S. H. Cho, K. L. Mulfort, D. M. Tiede, J. T. Hupp and S. B. T. Nguyen, *J. Am. Chem. Soc.*, 2008, **130**, 16828–16829.

34 P. Zhang, J. Meijide Suárez, T. Driant, E. Derat, Y. Zhang, M. Ménand, S. Roland and M. Sollogoub, *Angew. Chem., Int. Ed.*, 2017, **56**, 10821–10825.

35 R. Gramage-Doria, J. Hessels, S. H. A. M. Leenders, O. Tröppner, M. Dürr, I. Ivanović-Burmazović and J. N. H. Reek, *Angew. Chem., Int. Ed.*, 2014, **53**, 13380–13384.

36 Q.-Q. Wang, S. Gonell, S. H. A. M. Leenders, M. Dürr, I. Ivanović-Burmazović and J. N. H. Reek, *Nat. Chem.*, 2016, **8**, 225–230.

37 M. Guitet, P. Zhang, F. Marcelo, C. Tugny, J. Jiménez-Barbero, O. Buriez, C. Amatore, V. Mouriès-Mansuy, J.-P. Goddard, L. Fensterbank, Y. Zhang, S. Roland, M. Ménand and M. Sollogoub, *Angew. Chem., Int. Ed.*, 2013, **52**, 7213–7218.

38 S. S. Nurttila, W. Brenner, J. Mosquera, K. M. van Vliet, J. R. Nitschke and J. N. H. Reek, *Chem.–Eur. J.*, 2019, **25**, 609–620.

39 V. F. Slagt, P. W. N. M. van Leeuwen and J. N. H. Reek, *Angew. Chem., Int. Ed.*, 2003, **42**, 5619–5623.

40 P. Dingwall, J. A. Fuentes, L. Crawford, A. M. Z. Slawin, M. Bühl and M. L. Clarke, *J. Am. Chem. Soc.*, 2017, **139**, 15921–15932.

41 Y. H. Lam, M. N. Grayson, M. C. Holland, A. Simon and K. N. Houk, *Acc. Chem. Res.*, 2016, **49**, 750–762.

42 L. Xu, M. Hilton and X. Zhang, *J. Am. Chem. Soc.*, 2014, **136**, 1960–1967.

43 Y. Dang, S. Qu, Z. X. Wang and X. Wang, *J. Am. Chem. Soc.*, 2014, **136**, 986–998.

44 M. J. Hilton, L. P. Xu, P. O. Norrby, Y. D. Wu, O. Wiest and M. S. Sigman, *J. Org. Chem.*, 2014, **79**, 11841–11850.

45 T. Sperger, I. A. Sanhueza, I. Kalvet and F. Schoenebeck, *Chem. Rev.*, 2015, **115**, 9532–9586.

46 T. Sperger, I. A. Sanhueza and F. Schoenebeck, *Acc. Chem. Res.*, 2016, **49**, 1311–1319.

47 K. D. Vogiatzis, M. V. Polynski, J. K. Kirkland, J. Townsend, A. Hashemi, C. Liu and E. A. Pidko, *Chem. Rev.*, 2019, **119**, 2453–2523.

48 M. S. Sigman, K. C. Harper, E. N. Bess and A. Milo, *Acc. Chem. Res.*, 2016, **49**, 1292–1301.

49 A. R. Rosales, S. P. Ross, P. Helquist, P. O. Norrby, M. S. Sigman and O. Wiest, *J. Am. Chem. Soc.*, 2020, **142**, 9700–9707.

50 J. J. Dotson, L. van Dijk, J. C. Timmerman, S. Grosslight, R. C. Walroth, F. Gosselin, K. Püntener, K. A. Mack and M. S. Sigman, *J. Am. Chem. Soc.*, 2023, **145**, 110–121.

51 R. C. Cammarota, W. Liu, J. Bacsa, H. M. L. Davies and M. S. Sigman, *J. Am. Chem. Soc.*, 2022, **144**, 1881–1898.

52 J. Werth and M. S. Sigman, *J. Am. Chem. Soc.*, 2020, **142**, 16382–16391.

53 K. C. Harper, S. C. Vilardi and M. S. Sigman, *J. Am. Chem. Soc.*, 2013, **135**, 2482–2485.

54 C. Zhang, C. B. Santiago, L. Kou and M. S. Sigman, *J. Am. Chem. Soc.*, 2015, **137**, 7290–7293.

55 T.-S. Mei, H. H. Patel and M. S. Sigman, *Nature*, 2014, **508**, 340–344.

56 T. S. Mei, E. W. Werner, A. J. Burckle and M. S. Sigman, *J. Am. Chem. Soc.*, 2013, **135**, 6830–6833.

57 A. Milo, E. N. Bess and M. S. Sigman, *Nature*, 2014, **507**, 210–214.

58 A. Milo, A. J. Neel, F. D. Toste and M. S. Sigman, *Science*, 2015, **347**, 737–743.

59 A. F. Zahrt, J. J. Henle, B. T. Rose, Y. Wang, W. T. Darrow and S. E. Denmark, *Science*, 2019, **363**, 1–11.

60 D. T. Ahneman, J. G. Estrada, S. Lin, S. D. Dreher and A. G. Doyle, *Science*, 2018, **360**, 186–190.

61 R. Franke, D. Selent and A. Börner, *Chem. Rev.*, 2012, **112**, 5675–5732.

62 P. W. N. M. van Leeuwen, C. P. Casey and G. T. Whiteker, *Rhodium Catalyzed Hydroformylation*, Kluwer Academic Publishers, Dordrecht, 2000.

63 M. Kranenburg, Y. E. M. van der Burgt, P. C. J. Kamer, P. W. N. M. van Leeuwen, K. Goubitz and J. Fraanje, *Organometallics*, 1995, **14**, 3081–3089.

64 P. R. Linnebank, A. M. Kluwer and J. N. H. Reek, 2023, submitted.

65 I. Jacobs, B. de Bruin and J. N. H. Reek, *ChemCatChem*, 2015, **7**, 1708–1718.

66 P. R. Linnebank, A. M. Kluwer and J. N. H. Reek, *ChemCatChem*, 2022, **14**, e202200541.

67 B. Breit, *Top. Curr. Chem.*, 2007, **279**, 139–172.
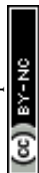
68 B. Breit and W. Seiche, *Synthesis*, 2001, 1–36.

69 Z. Yu, M. S. Eno, A. H. Annis and J. P. Morken, *Org. Lett.*, 2015, **17**, 3264–3267.

70 Z.-M. Chen, M. J. Hilton and M. S. Sigman, *J. Am. Chem. Soc.*, 2016, **138**, 11461–11464.

71 G. te Velde, F. M. Bickelhaupt, E. J. Baerends, C. Fonseca Guerra, S. J. A. van Gisbergen, J. G. Snijders and T. Ziegler, *J. Comput. Chem.*, 2001, **22**, 931–967.

72 E. J. Baerends, T. Ziegler, J. Autschbach, D. Bashford, A. Bérces, F. M. Bickelhaupt, C. Bo, P. M. Boerrigter, L. Cavallo, D. P. Chong, L. Deng, R. M. Dickson, D. E. Ellis, M. van Faassen, L. Fan, T. H. Fischer, C. Fonseca Guerra, M. Franchini, *ADF2017, SCM, Theoretical Chemistry*, Vrije Universiteit, Amsterdam, The Netherlands, 2017.

73 C. Fonseca Guerra, J. G. Snijders, G. te Velde and E. J. Baerends, *Theor. Chem. Acc.*, 1998, **99**, 391–403.

74 S. Grimme, S. Ehrlich and L. Goerigk, *J. Comput. Chem.*, 2011, **32**, 1456–1465.

75 S. Grimme, J. Antony, S. Ehrlich and H. Krieg, *J. Chem. Phys.*, 2010, **132**, 154104.

76 A. D. Becke, *J. Chem. Phys.*, 1993, **98**, 1372–1377.

77 L. Dixit, *Appl. Spectrosc. Rev.*, 1984, **20**, 159–254.

78 A. Verloop, in *Drug Design*, Academic Press, New York, 1976.

79 *RDKit: Open-Source Cheminformatics Software*, http://www.rdkit.org, accessed Jan 2023.

80 L. B. Kier and L. H. Hall, Derivation and Significance of Valence Molecular Connectivity, *J. Pharm. Sci.*, 1981, **70**, 583–589.

81 L. H. Hall and L. B. Kier, *Rev. Comput. Chem.*, 2007, **2**, 367–422.

82 P. Ertl, in *Molecular drug properties*, 2007, pp. 111–126.

83 M. Petitjean, Applications of the Radius-Diameter Diagram to the Classification of Topological and Geometrical Shapes of Chemical Compounds, *J. Chem. Inf. Comput. Sci.*, 1992, **32**, 331–337.

84 N. C. Firth, N. Brown and J. Blagg, *J. Chem. Inf. Model.*, 2012, **52**, 2516–2525.

85 R. Todeschini and V. Consonni, in *Handbook of Chemoinformatics*, Wiley-VCH Verlag GmbH, Weinheim, Germany, 2008, pp. 1004–1033.

86 C. Fonseca Guerra, J. W. Handgraaf, E. J. Baerends and F. M. Bickelhaupt, *J. Comput. Chem.*, 2004, **25**, 189–210.